Photolithography reaches 6 nm half-pitch using extreme ultraviolet light

Daniel Fan* **and Yasin Ekinci**
Paul Scherrer Institut, Laboratory for Micro and Nanotechnology, Villigen-PSI 5232, Switzerland

Abstract. Extreme ultraviolet interference lithography records the interference pattern of two diffracted, coherent light beams, where the pattern resolution is half the diffraction grating resolution. The fabrication of diffraction grating masks by e-beam lithography is restricted by the electron proximity effect and pattern transfer limitations into diffraction efficient materials. By patterning HSQ lines at a relaxed pitch to avoid the electron proximity effect, depositing conformal iridium via atomic layer deposition, followed by ion milling the top and bottom iridium and HSQ removal, we fabricated iridium diffraction gratings at double the line spacing of the original HSQ lines. Line/space patterns of 6-nm half-pitch patterns were achieved using these masks, marking a new record resolution in photolithography. [DOI: 10.1117/1.JMM.15.3.033505]

Keywords: line doubling; spatial frequency doubling; extreme ultraviolet; interference lithography; high-resolution; diffraction grating.

Paper 16073P received May 11, 2016; accepted for publication Jul. 12, 2016; published online Aug. 1, 2016.

1 Introduction

The feature sizes of microelectronic devices have been steadily decreasing as guided by Moore's law. To further extend this downscaling, new top-down patterning methods need to be explored.[1] One candidate technology is extreme ultraviolet (EUV) lithography at the source wavelength of 13.5 nm.[2] Using a shorter wavelength compared to deep UV allows a corresponding increase in resolution. As EUV technology undergoes further research and development to prepare it for industrial use, EUV interference lithography (IL) has been used for the research and development of suitable photoresists, since EUV-IL is capable of printing the highest resolution patterns possible using photon-based sources.[3] Furthermore, EUV-IL is capable of printing high-resolution, highly dense periodic patterns over a large area with high throughput in comparison to other research tools such as e-beam lithography, allowing the fabrication of nanoscale structures for scientific study of, e.g., nanocatalysis,[4] magnetic frustration,[5] metal nanostructures,[6] and quasicrystallinity.[7]

The XIL-II beamline at the Swiss Light Source (SLS), Paul Scherrer Institut (PSI), hosts a broadband EUV beam with high spatial coherence and low emittance and an interferometric tool where periodic patterns of holes, dots, and lines and spaces with feature sizes of 10 nm half-pitch (HP) can be reached regularly[8] and resolution down to 7 nm HP is demonstrated.[9] Further increase in the resolution will severely test the capabilities of the beamline experimental setup, the characteristics of high-resolution EUV photoresists,[10] and the fabrication of high quality IL masks. In the first case, the effect of source extension and of mechanical vibrations plays a role in resolution improvement and limitations. For photoresists, their homogeneous application, adhesion, and process optimization become critically important. The fabrication of diffraction efficient gratings on the IL mask also presents a significant challenge.[11]

In this work, we show patterning of 6-nm HP line/space patterns by optimizing the mask fabrication. Spatial line doubling of the mask grating using EUV diffraction efficient material (iridium) was used to fabricate an effective mask. Such a feature size represents ~12 atoms of silicon in width, and it is well within the quantum regime where quantum effects play an important role in device physics. For EUV-IL, 6-nm HP is close to the theoretical limit of ~3.5-nm HP for this scheme. The result is an improvement on the previous 7-nm HP patterning using Inpria-based photoresist as the mask grating,[9] and as far as the authors are aware, represents the highest resolution achieved to date using photolithography.

2 Theory

The basic principle of IL is shown in Fig. 1 and is described elsewhere in detail.[3] Briefly, two (or more) coherent light waves interfere and this interference pattern is recorded in photoresist. Generation of the coherent beams can be accomplished by using Lloyd's mirrors,[12] prisms, or diffraction gratings,[3] and requires a coherent source. The benefit of diffraction gratings is that temporal coherence can be relaxed as different wavelengths lead to the same aerial image as will be discussed later. Disadvantages include difficulties in fabrication of diffraction masks with high-resolution, low roughness, and high diffraction efficiency. Using IL, high-resolution periodic patterns can be produced without optics.

Considering Fig. 1, the incident beam λ is diffracted by gratings of period q through an angle θ for the diffraction order m, and following the Bragg equation, leads to the interference pattern with the period p[3]

$$p = \frac{\lambda}{2 \sin \theta} = \frac{q}{2m}. \quad (1)$$

Therefore, the periodicity of the aerial image is half the periodicity of the diffraction grating for the first-order

*Address all correspondence to: Daniel Fan, E-mail: daniel.fan@psi.ch

1932-5150/2016/$25.00 © 2016 SPIE

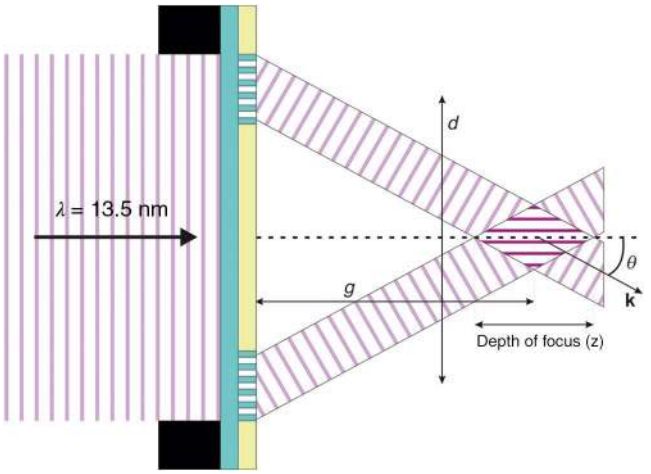

Fig. 1 EUV IL scheme. EUV light illuminates a transmission mask from the left. The mask consists of gratings which diffract the coherent beam, and elsewhere areas where the light is prevented from transmission. The diffracted coherent beams form an interference pattern which is recorded in photoresist.

diffraction and the absolute limit in resolution, corresponding to a diffraction angle of 90 deg, is an HP of $\lambda/4$, resulting in about 3.4 nm for EUV. At resolutions lower than this wavelength limit, the resolution achievable by IL is directly related to the resolution obtainable for writing the mask diffraction grating. The location of the aerial interference image, or mask-to-sample gap, g, is given as

$$g = \frac{d}{2 \tan \theta}, \tag{2}$$

where d is the distance between the centers of the two diffraction gratings (Fig. 1). This distance must be greater than the diffraction grating field area, so that the zeroth-order transmitted light from the grating does not overlap the interference area, and it must be smaller than the beam spot size so that all the incoming light is incident upon the gratings. The zeroth-order transmitted light elsewhere is blocked. We note that the optimal gap defined in Eq. (2) enables the maximum overlap of two interfering beams and thereby maximizes the total area of the aerial image, but it has no effect on the contrast of the aerial image, therefore, IL has infinite depth-of-focus.

The diffraction efficiency of the grating at EUV wavelengths is an important consideration in IL. Sufficient diffracted light must be available such that recording of the aerial image can occur in a reasonable exposure time to mitigate mechanical instabilities. As the wavelength of incident light becomes similar in scale to the diffraction grating period, the scalar approximation of the far-field transmitted image is no longer valid, and to calculate the diffraction efficiency rigorous methods must be used.[13] Boundary effects due to the grating material must be taken into account, and Maxwell's equations must be used fully. We used the rigorous coupled wave analysis (RCWA) method, a semianalytical method derived directly from Maxwell's equations, suitable for solving light propagation through periodic media.[14]

The diffraction efficiency of gratings of various materials, given their refractive indices at EUV,[15] was calculated for gratings with different duty cycles and thicknesses up to 200 nm using RCWA.[16] The number of diffraction modes to be calculated was set high enough to ensure convergence of the solution. The maximum diffraction efficiency available for each grating period, for any duty cycle and grating height up to 200 nm, was plotted in Fig. 2(a). Grating thicknesses above 200 nm were deemed too difficult to fabricate as the large aspect ratios would cause grating collapse. Traditionally, for soft x-ray optics, metals such as gold, chromium, and nickel[17] are used as the grating material.

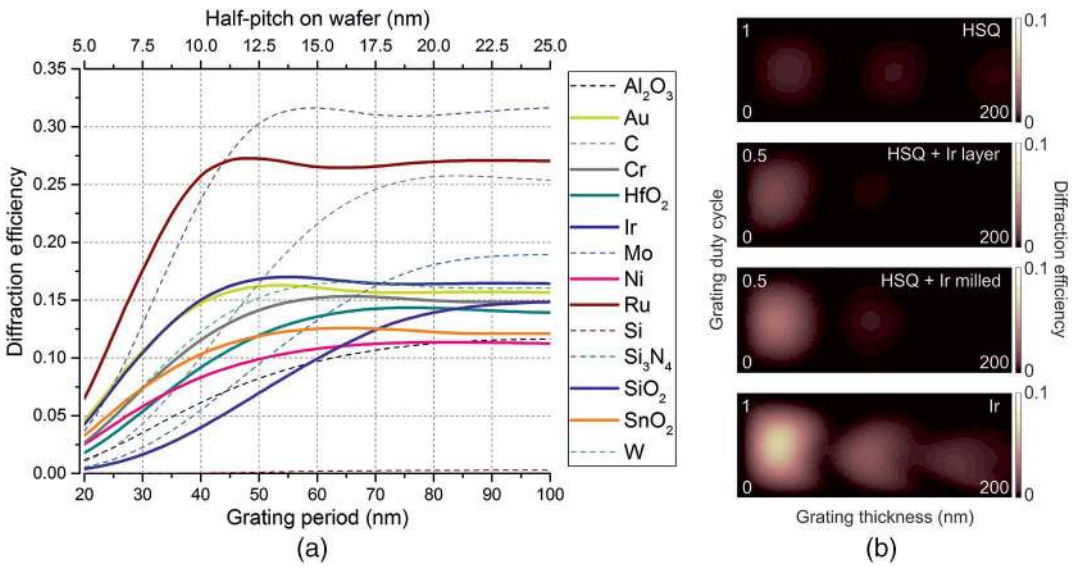

Fig. 2 (a) RCWA simulation of the highest available diffraction efficiency for gratings of various materials and grating periods, for gratings with a height between 0 and 200 nm, and a duty cycle between 0 and 1. The top axis represents the equivalent HP of the interference pattern. (b) RCWA simulations of gratings composed of HSQ at 24 nm period, HSQ at 48 nm period with a 12-nm conformal Ir layer, HSQ at 48 nm period with the conformal Ir at the top and bottom of the grating ion milled away, and an Ir grating at 24 nm period. All gratings target an interference pattern with 6-nm HP.

Table 1 EUV ($\lambda = 13.5$ nm) IL mask design parameters.

Targeted HP on sample wafer (p)	6 nm	Mask grating HSQ period (q)	48 nm
Mask to sample gap (g)	150 μm	HSQ line-width	12 nm
Distance between gratings (d)	204.1 μm	Ir deposition	12 nm
Diffraction angle (θ)	34.2 deg	Grating field size	50 μm $\times$ 50 μm

For grating periods above 80 nm such metals are straightforward to pattern transfer via electroplating or reactive ion etching. Below 50 nm periods however, pattern transfer into such metals becomes challenging due to the high resolutions involved. One alternative method used with success for grating periods between 40 and 80 nm is direct writing of gratings using hydrogen silesquoxiane (HSQ) photoresist[11] by electron-beam lithography. HSQ is a high-resolution negative-tone resist which becomes a form of SiO_2 after development. Although this greatly simplifies the patterning process, below a 40 nm grating period the diffraction efficiency of SiO_2 drops significantly [Fig. 2(a)].

One way to avoid pattern transfer while still giving high diffraction efficiencies is to use high-resolution photoresists based on highly absorbing materials such as HfO_2.[9] Directly written gratings of HfO_2 and SnO_2 enable relatively high diffraction efficiencies compared to HSQ. However, with increasing resolution pattern collapse limits the achievable aspect ratio and thereby limits the diffraction efficiencies. Furthermore, at high resolutions, the electron proximity effect in e-beam lithography comes into play, and the writing of smooth, high-resolution lines becomes increasingly difficult. The record achievable grating periods at the Laboratory for Micro and Nanotechnology (LMN), PSI for the various processing methods, as well as the corresponding HP on the sample wafer following IL that has been successfully achieved, are as follows: using e-beam written HSQ gratings, period 40 nm and above, 10 nm HP on wafer;[18] for molybdenum gratings with pattern transfer via RIE, period 64 nm, 8 nm HP on wafer using second-order diffraction;[19] for e-beam written HfO_2-based gratings, period 28 nm, 7 nm HP on wafer;[9] for e-beam written SnO_2-based gratings, period 28 nm, 7 nm HP on wafer.[20] To extend the resolution limit of grating fabrication, various approaches can be used. Ion milling can be used as the pattern transfer method into diffraction efficient materials, with the benefit of high anisotropy and relatively stable etch rates for different materials compared to reactive ion etching. The disadvantage is that the diffraction grating pattern is still written by e-beam lithography and is thus still susceptible to electron proximity effect.

The approach presented in this work is to achieve high-resolution gratings by doubling the grating line frequency using atomic layer deposition (ALD) for conformal deposition of a diffraction efficient material. A sparse grating with 25% duty cycle and a period double the targeted period, which in this case is 48 nm period with 12 nm line-width, is written using e-beam lithography in HSQ. Because of the sparseness, the proximity effect becomes less noticeable and smooth lines can be written. Next, conformal deposition of 12 nm of iridium (Ir), which has relatively high diffraction efficiency at EUV as shown in Fig. 2(a), is performed using ALD. Other candidate materials include aluminum oxide (Al_2O_3) which can be deposited very smoothly but has a lower diffraction efficiency than iridium, and ruthenium (Ru) which has higher diffraction efficiency than iridium but cannot be deposited smoothly without extensive process optimization. The top and bottom Ir are removed by ion milling, which is highly anisotropic and therefore leaves the Ir layer on the sidewalls of the HSQ. The spatial line frequency has thus been effectively doubled from the original 48 to 24 nm.

Finally, the HSQ in between the Ir lines can be removed to further improve the diffraction efficiency. Simulations of the various gratings after each processing step are shown in Fig. 2(b), all targeting 6-nm HP on wafer. A purely HSQ grating with a 24 nm period shows relatively low diffraction efficiency [Fig. 2(b), top]. By writing a sparse 48-nm period HSQ grating followed by ALD of Ir, the diffraction efficiency can be improved as seen in Fig. 2(b), second top. Further ion milling improves the efficiency again, while removal of the HSQ improves the efficiency up to 10% [Fig. 2(b), bottom]. Also note that the most efficient geometry is for a 25% duty cycle HSQ grating at a height of ~35 nm. As ALD can be optimized to achieve good smoothness, the pattern transfer limitations of electroplating and etching can be avoided, while a highly diffraction efficient material can be used. The limitation of e-beam lithography in achieving dense lines is circumvented by writing a sparse grating. The process window in terms of tolerances in the grating geometry can also be seen to be fairly relaxed [Fig. 2(b)]: an Ir grating with 40% to 60% duty cycle and height from 30 to 40 nm can achieve relatively high diffraction efficiency. Therefore, slight errors in the mask fabrication process can be tolerated. A summary of the mask design is shown in Table 1. The mask-to-sample gap, g, was kept as small as possible to reduce the blur due to source extension, while being large enough to ensure mechanical positioning tolerances.

3 Fabrication of Extreme Ultraviolet-Interference Lithography Masks

A 100-nm-thick silicon nitride membrane with a 3×3 mm^2 window was used as the grating support (mask). The silicon nitride was thermally grown (Center of MicroNanoTechnology CMi, EPFL, Lausanne, Switzerland) on a silicon substrate and the mask window fabricated at the LMN, PSI using standard lithography and etching processes. Gold markers were fabricated on the mask frame using e-beam lithography outside the mask window to facilitate alignment for subsequent overlaid e-beam exposures. A short oxygen plasma treatment (RIE 80, Oxford Instruments, UK) was used at 150 W for

30 s to clean the surface of the membrane and to improve the hydrophilicity for better adhesion of the subsequent photoresist application. The mask was placed on a spin-coating chuck with a small droplet of deionized (DI) water underneath the mask window for support. Next, HSQ (XR1541, Dow Chemical, Midland, Michigan) was spin-coated at 5000 rpm for 45 s for a thickness of ~35 nm. The designed diffraction gratings of line-width 12 nm and period 48 nm were written using e-beam (VISTEC EBPG 1000+, Jena, Germany) at a dose between 12,000 and 14,000 $\mu C/cm^2$, using a 1-nA current beam with 200-μm aperture, giving a spot size of ~3.5 nm. No metallic thin film was used, as the electron conduction was found to be sufficient for high-resolution writing. The mask was then developed in a NaOH-buffered solution (Microposit 351, Dow Chemical) diluted 1:3 with DI water for 30 s, producing gratings of SiO_2-based material, at a height slightly less than the spin-coated thickness due to resist shrinkage after development. HSQ is an excellent high-resolution photoresist suitable for electron- and photon-based exposure. The negative-tone cross linking gives HSQ, after development, a profile with slightly positively sloped sidewalls. The SiO_2-based material can be removed by fluorine-based etchants but otherwise is very stable.

A second pattern is then written for the fabrication of the photon-stop to prevent the transmission of zeroth-order light. The mask is placed again on a spin-coating chuck with a droplet of DI water to support the mask window. Poly methyl acrylate (PMMA, molecular weight 950k, Allresist GmbH, Strausberg, Germany) dissolved 4% in ethylactate (Technic France, Saint-Denis, France) was spin-coated at 2000 rpm for 45 s to target a thickness of ~400 nm to be used as a positive tone photoresist, followed by a post application bake at 175°C for 5 min. After alignment, all areas of the mask except the grating areas were exposed at a dose of 1000 $\mu C/cm^2$ using a 190-nA current beam. The mask was then developed in isopropanol (Technic France) mixed 7:3 with DI water for 10 s to leave PMMA covering the grating areas on the mask. Thermal evaporation of 5 nm of chromium for adhesion, followed by 10 nm of gold as electroplating seed layer, was performed (Balzers, Oerlikon, Liechtenstein). The mask was then placed in acetone (Technic France) overnight to lift-off the PMMA covered areas, i.e., the grating areas, which are left without any electroplating seed layer. Very light agitation with a small syringe was performed by hand to facilitate the lift-off. The mask then underwent nickel electroplating in a nickel sulfamate/boric acid based bath (Lectro-nic 10-03, Ethone, West Haven, Connecticut) using monophasic pulses of ~2.5 mA/cm^2 current density, 67% duty cycle, and 2 s cycle time, for an overall plating time of 7 min to target a nickel thickness of ~400 nm. This thickness was calculated using the absorption coefficient of nickel at EUV radiation[15] to be sufficient to effectively block EUV light. The electroplating parameters were optimized[21] to minimize stress on the membrane and ensure relatively homogeneous electroplating across the desired area.

The mask, which now consists of HSQ-based gratings of 48 nm period and 12 nm line-width surrounded by 400-nm thick nickel, is then coated with conformal Ir using ALD (Picosun, Espoo, Finland) at 270°C. Plasma-enhanced ALD was used with the Ir precursor Ir(III) 2,4-pentanedionate [Ir(acac)3, abcr GmbH, Karlsruhe, Germany] combined with pulses of oxygen plasma to improve the smoothness of the deposited film and decrease the grain size. A complete cycle (1 s on, 2 s purge, 1 s on, 2 s purge, 1 s on, 6 s purge, oxygen plasma 2 s on at 2000 W, 6 s purge) was measured to deposit at a rate of 0.243 Å/cycle. The seed time or initial cycles needed to begin the deposition was measured to be three cycles. Plasma enhancement in the ALD cycle improves the surface smoothness,[22,23] especially important when depositing a thin film which needs to be as smooth as possible. 506 cycles were performed targeting 12 nm of iridium deposition. Finally, the mask was ion milled (Ionfab 300Plus, Oxford Instruments, UK) to remove the top and bottom iridium while leaving the sidewall iridium intact. Ar ion milling is highly anisotropic with a relatively slow etching rate compared to RIE, while care must be taken with regards to redeposition of the etched material. A plasma with power 150 W, grid voltage of 400 V, and gun current of 4.5 mA was used to give an etch rate of 1 nm/min. The etch time was 9 min targeting an etch of 9 nm of Ir. The Ar flow rate was 8 sccm and the sample held at 20°C. The completed mask was then mounted on a stainless steel mask holder using PMMA and the completed assembly installed in the XIL beamline for the IL. The complete process flow is summarized in Fig. 3.

Figure 4 shows the diffraction grating on the mask under scanning electron microscopy (SEM, ZEISS Supra, Jena, Germany) after (a) and (b) iridium deposition and (c) ion milling. First, the dimensions of the grating are slightly different from the targeted dimensions. The HSQ lines appear slightly smaller because of the positive slope of the negative-tone resist such that the line is narrower on top, and also

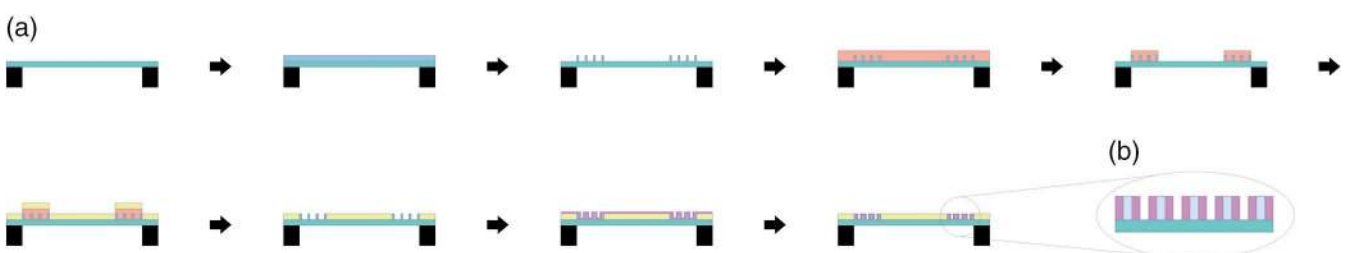

Fig. 3 Mask fabrication process flow. An SiN membrane is spin-coated with HSQ and a sparse grating written using e-beam. A second e-beam overlay in PMMA followed by metal deposition, lift-off, and nickel electroplating produces the photon stop. Finally, iridium is deposited by ALD and then ion milled to remove the top and bottom iridium, leaving an iridium grating with double the spatial line frequency of the original HSQ grating.

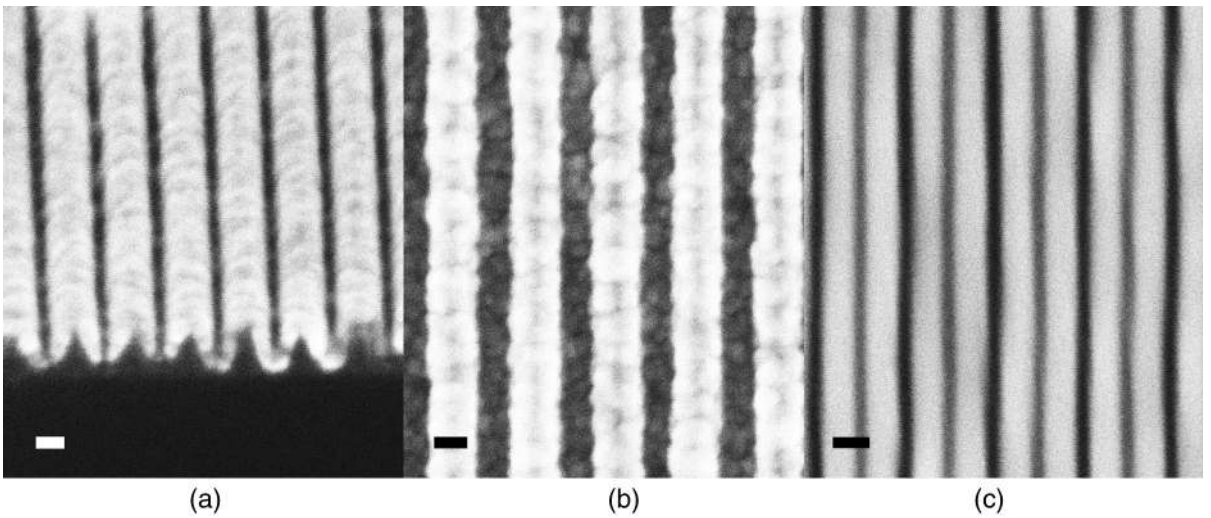

Fig. 4 SEM of 48 nm period 12 nm line-width HSQ grating (dark) with 12 nm iridium deposited on top via ALD (bright) (a) cross-sectional view and (b) top view. (c) After ion milling, top view. The bright areas show iridium, the light dark area is the HSQ while the dark area is empty. Scale bars equal 20 nm.

because of resist shrinkage of ∼1 nm after development. The Ir layer looks slightly larger than targeted due to the increased brightness under SEM inspection, as well as inhomogeneous grain sizes. Nevertheless, as can be seen from simulations, the window of grating dimensions which still allow reasonable diffraction efficiency is sufficiently large, therefore, some errors in the grating geometry can be tolerated. Finally, it can be noted from Fig. 4(c) that ion milling has the added benefit of smoothing the sidewalls and grains of the Ir layer, giving much smoother grating lines. Note that we only milled 9 nm of Ir from the line-doubled grating, and the HSQ has not been removed. This is for practical reasons, as the yield for such a mask-making process is rather low, and to avoid pattern collapse of the structure it was decided not to fully etch the Ir lines and perform the HF dip necessary to remove the HSQ. The mask diffraction efficiency can be improved by performing these processes.

4 Extreme Ultraviolet Exposures

EUV radiation was provided by a third-generation 2.4 GeV synchrotron source (SLS, PSI, Switzerland). A linear undulator with a periodic arrangement of 22 permanent magnet pairs and adjustable gap can provide an EUV beam with energies between 70 and 500 eV. The beam passes through three mirrors in order to filter the higher harmonics and is focused to a pinhole of 70 μm diameter which serves as the effective intermediate source. The beam is polarized along the gratings, providing the maximum contrast for line/space patterns. The exposure chamber incorporating the mask holder and the sample stage is placed 12 m away from the pinhole, with the beam having a spot size of 1.2×1.8 mm^2 on the mask. The beamline arrangement is shown in Fig. 5. From the geometrical arrangement of the experimental setup, the blur due to extended source was calculated to be ∼1 nm, which is not negligible for the targeted 6-nm HP resolution.

The sample to be patterned, a 550-μm-thick ⟨100⟩ single-side polished silicon wafer, was dipped in a solution of a tetramethylammonium hydroxide-based developer MF26A (Dow Chemical) for 60 s followed by rinsing in DI water for 60 s, nitrogen blow dry, then baking on a hotplate at 180°C for 5 min. This pretreatment is used to promote adhesion of the photoresist. Other methods for adhesion promotion include using a light powered oxygen plasma and/or baking the wafer at 250°C for 5 min. These treatments improve the hydrophilicity of the wafer surface. Next, HSQ negative-tone photoresist XR1541 diluted 1:1 with methyl isobutyl ketone solvent (MIBK, Dow Chemical) was spin-coated at 2500 rpm to target a thickness of

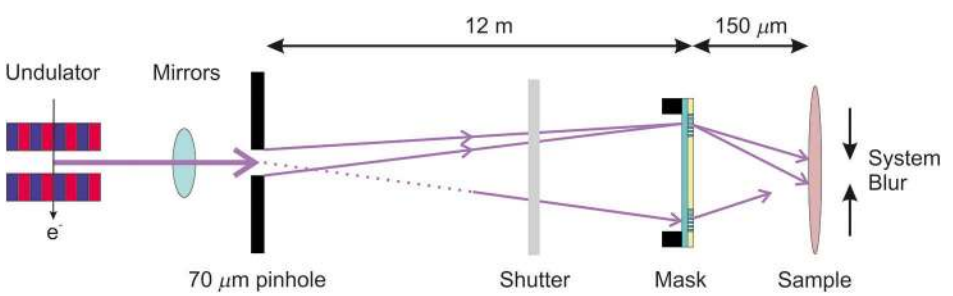

Fig. 5 Schematic of the XIL-II beamline at the SLS, PSI. The violet arrows represent the EUV beam path. After being produced in the undulator, the beam passes through a set of mirrors acting as harmonic filters. A 70-μm pinhole is used for spatial filtering and acts as the effective source. The mask/sample arrangement is placed 12 m away, producing a blur of ∼1 nm.

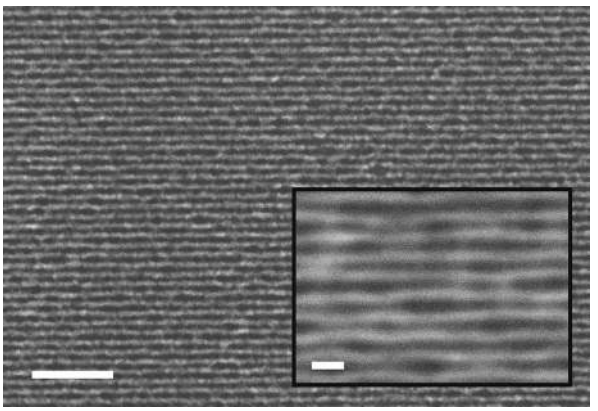

Fig. 6 A 6-nm HP pattern produced by EUV-IL onto HSQ photoresist. Scale bar is 100 nm. Inset scale bar 20 nm.

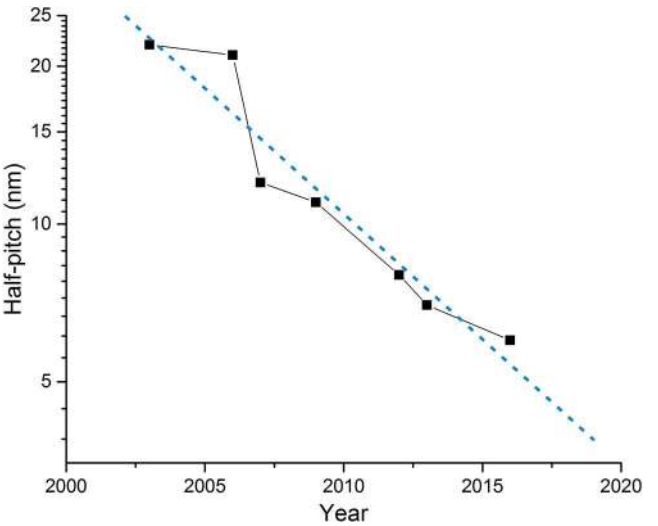

Fig. 7 Progression of minimum achievable HP in nm using the XIL-II tool at the SLS, PSI.

~20 nm. Higher spin speeds were previously shown to result in inhomogeneous resist layer thickness or even complete lack of adhesion. The sample wafer was mounted onto the motorized sample stage and the exposure performed using radiation at 92 eV (13.5 nm) with a photon flux of ~30 mW/cm^2. The dose was varied from 4000 to 8000 mJ/cm^2, corresponding to exposure times between 2 and 4 min. The sample was then developed in NaOH-buffered developer (Microposit 351) mixed 1:3 with DI water for 30 s, rinsed under DI water for 60 s, and blow dried using nitrogen. The sample was finally inspected using SEM at an acceleration voltage of 1 kV and working distance of 3.5 mm.

The results are shown in Fig. 6. Line/space patterns with 6-nm HP were resolved in HSQ at an aspect ratio of ~3:1, although bridging and collapse were evident. The SEM images were analyzed using a metrology software package (SuMMIT, EUV Tech, Martinez, California) which calculated a pitch of 12.245 nm with a critical dimension of 5.7 nm and duty cycle of 0.458. The mask incorporated only this HP due to the fabrication process, which can be optimized to only a single HP. The exposure dose was 7500 mJ/cm^2 corresponding to 125 s of exposure time. Although the pattern is well-resolved, it shows significant bridging between the lines and partial pattern collapse. It seems that we are at the resolution limit with this approach. This could be due to a variety of reasons including mask fabrication (e.g., line edge roughness of the mask), resist processing (pattern collapse, resolution limit of the resist), or tool limitations (e.g., mechanical instabilities during the exposure). At this point, it is difficult to isolate the root cause of the problem because masks fabricated using this method can only target one HP, making it difficult to compare with different resolution patterns on the same mask to determine if there are mask defects. Moreover, there is no immediate possibility of comparing results with any other resist or tool, since both HSQ and the XIL-II tool have the best performance in terms of resolution.

Future work will include further optimization of the mask fabrication process including, for instance, further ion milling to completely remove the remaining top and bottom Ir and removal of the HSQ. With regards to the photoresist application onto the sample wafer, adhesion could be possibly enhanced by pretreatment with oxygen plasma or baking of the sample. Further, the resist thickness could be decreased to decrease the final aspect ratio by thinning the HSQ further with MIBK. It must be noted that HSQ is particularly sensitive to humidity, temperature, and age, and incorrect handling may also be a contributing factor toward suboptimal results. Finally, the system blur due to source extension can be decreased by using a smaller pinhole at the intermediate focus. This would, however, lower the available flux and thereby increase exposure times, causing the exposure to be more sensitive to mechanical instabilities. Pattern collapse mitigation techniques such as critical point drying can be used in order to remove the limitation of pattern collapse.

5 Conclusions

We show patterning of line/spaces with an HP of 6 nm using HSQ photoresist via IL. The high-resolution mask was fabricated by writing a sparse HSQ grating using e-beam lithography to avoid proximity effect errors, followed by ALD of conformal iridium to effectively double the line frequency of the written grating. Iridium was chosen due to its smooth deposition and good diffraction efficiency at EUV wavelengths. RCWA simulations show a fair tolerance window in grating geometry which gives reasonable diffraction efficiency. The interference exposure yielded well-resolved dense resist patterns with 6-nm HP, although pattern collapse and bridging was evident. The resolution limit could be due to the mask, resist, resist processing, or tool limits. Further process optimization can be expected to improve the line edge roughness, although achieving higher resolution becomes more and more difficult due to a combination of lower diffraction efficiencies and thus longer exposure times, the effect of source extension, and diffraction gratings having higher required tolerances.

With 6-nm HP resolution, we have achieved a new milestone in our progress with EUV IL. Figure 7 shows the resolution limit of the IL tool at the SLS, PSI, demonstrated over the years. Steady process has been made for producing high-resolution patterns, giving access to high contrast, high-resolution, and well-defined aerial images for the early development of photoresists for EUV lithography. The 6-nm HP marks a new record in photolithography, which is

a remarkable achievement. The 6-nm HP corresponds in width to ∼12 silicon atoms or ∼18 silicon oxide molecules. It is a significant demonstration that EUV photons can achieve such a resolution. The secondary electron blur for EUV is estimated to be 1 to 3 nm.[24] If, in reality, this is about 3 nm, we have probably reached the ultimate limit in photolithography. If the secondary electron blur is lower, the resolution might be further increased down to 5 nm HP. For high volume manufacturing (HVM), EUV scanners with 0.55 NA optics might be able to achieve 6-nm HP resolution.[25] This requires suitable photoresists with much higher sensitivity than that of HSQ.

In order to achieve beyond this resolution, the wavelength should be reduced. We have tried patterning with BEUV (6.5 nm wavelength) and with soft x-rays.[11] The advantage of reduced wavelength comes along with significant technological challenges. Moreover, secondary electron blur will probably increase with any further decrease in wavelength. Therefore, we do not expect better resolution at these short wavelengths. One feasible option would be to decrease the wavelength to 12.5 nm, which is very close to the absorption edge of silicon (12.5 nm, 100 eV). This wavelength provides 7% improvement in resolution for the same NA and without changing materials for the resists or optics. In case free electron lasers are used for HVM in the future as proposed,[26] this wavelength, which can be called EUV+, would provide a feasible improvement in resolution without any change except changes in the period of the Mo/Si multilayers which also have a high reflectivity.[15] These improvements will mark the ultimate resolution in photolithography of 5 to 6 nm HP. Beyond this limit, top-down resolution can be pushed further using pattern multiplication techniques such as directed self-assembly and line doubling with ALD which is similar to the method that we employ in order to overcome the resolution limitation of e-beam lithography.

Acknowledgments

The authors would like to thank Michaela Vockenhuber for help with the interference lithography setup, Dr. Tero Kumala for performing the ion milling, and the late Dr. Jeroen Bosgra for optimization of the Ir PEALD process. We dedicate this work to the memory of Jeroen, who sadly passed away in 2015, at the age of 34. Part of the experimental work was performed at the Swiss Light Source, Paul Scherrer Institut. Funding was kindly provided by the Swiss National Science Foundation (SNF: 200021_143969).

References

1. ITRS, "International technology roadmap for semiconductors 2013 report," 2014, http://www.itrs.net (7 October 2015).
2. G. Tallents, E. Wagenaars, and G. Pert, "Optical lithography: lithography at EUV wavelengths," *Nat. Photonics* **4**, 809–811 (2009).
3. N. Mojarad, J. Gobrecht, and Y. Ekinci, "Interference lithography at EUV and soft x-ray wavelengths," *Microelectron. Eng.* **143**(C), 55–63 (2015).
4. W. Karim et al., "High-resolution and large-area nanoparticle arrays using EUV interference lithography," *Nanoscale* **7**(16), 7386–7393 (2015).
5. L. Wang et al., "Generation of high-resolution kagome lattice structures using extreme ultraviolet interference lithography," *Appl. Phys. Lett.* **101**, 093104 (2012).
6. J. Huang et al., "Fabrication of ultrahigh resolution metal nanowires and nanodots through EUV interference lithography," *Microelectron. Eng.* **41**(C), 32–36 (2015).
7. A. Langner et al., "Fabrication of quasiperiodic nanostructures with EUV interference lithography," *Nanotechnology* **23**, 105303 (2012).
8. B. Päivänranta et al., "Sub-10 nm patterning using EUV interference lithography," *Nanotechnology* **22**, 375302 (2011).
9. N. Mojarad et al., "Single-digit-resolution nanopatterning with extreme ultraviolet light for the 2.5 nm technology node and beyond," *Nanoscale* **7**(9), 4031–4037 (2015).
10. E. Buitrago et al., "Evaluation of EUV resist performance using interference lithography," *Proc. SPIE* **9422**, 94221S (2015).
11. N. Mojarad et al., "Broadband interference lithography at extreme ultraviolet and soft x-ray wavelengths," *Opt. Lett.* **39**(8), 2286–2289 (2014).
12. S. Prezioso et al., "A study of the mechanical vibrations of a table-top extreme ultraviolet interference nanolithography tool," *Rev. Sci. Instr.* **81**(4), 045110 (2010).
13. J. Goodman, *Introduction to Fourier Optics*, 2nd ed., McGraw-Hill, New York (1996).
14. T. Gaylord and M. Moharam, "Rigorous coupled-wave analysis of planar-grating diffraction," *J. Opt. Soc. Am.* **71**, 811–818 (1981).
15. E. Gullikson, "Index of refraction," The Center for X-Ray Optics (1995) http://henke.lbl.gov/optical_constants/getdb2.html (7 March 2016).
16. "Distribution page of Rodis," Universiteit Gent (2003) http://photonics.intec.ugent.be/research/facilities/design/rodis (7 March 2016).
17. E. M. Di Fabrizio et al., "High-efficiency multilevel zone plates for keV x-rays," *Nature* **401**(6756), 895–898 (1999).
18. R. Fallica, E. Buitrago, and T. Kulmala, (2015), unpublished raw data.
19. L. Wang et al., "Nearly amorphous Mo-N gratings for ultimate resolution in extreme ultraviolet interference lithography," *Nanotechnology* **25**(23), 235305 (2014).
20. E. Buitrago et al., "SnOx high-efficiency EUV interference lithography gratings towards the ultimate resolution in photolithography," *Microelectron. Eng.* **155**, 44–49 (2016).
21. K. Hili et al., "Nickel electroplating for high-resolution nanostructures," *Microelectron. Eng.* **141**(C), 122–128 (2015).
22. H. B. Profijt et al., "Plasma-assisted atomic layer deposition: basics, opportunities, and challenges," *J. Vac. Sci. Technol. A* **29**(5), 050801 (2011).
23. T. Hatanpaa, M. Ritala, and M. Leskela, "Precursors as enablers of ALD technology: contributions from University of Helsinki," *Coord. Chem. Rev.* **257**(23–24), 3297–3322 (2013).
24. A. Narasimhan et al., "Studying secondary electron behavior in EUV resists using experimentation and modeling," *Proc. SPIE* **9422**, 942208 (2015).
25. J. Van Schoot et al., "EUV lithography scanner for sub 8 nm resolution," *Proc. SPIE* **9422**, 94221F (2015).
26. A. Endo, "Optimization of high average power FEL beam for EUV lithography," *Proc. SPIE* **9512**, 95121O (2015).

Biographies for the authors are not available.